Ballast fouling inspection and quantification with ground penetrating radar (GPR)

Guo, Yunlong; Liu, Guixian; Jing, Guoqing; Qu, Jianjun; Wang, Shilei; Qiang, Weile

DOI
10.1080/23248378.2022.2064346

Publication date
2022

Document Version
Final published version

Published in
International Journal of Rail Transportation

International Journal of Rail Transportation

ISSN: (Print) (Online) Journal homepage: https://www.tandfonline.com/loi/tjrt20

Ballast fouling inspection and quantification with ground penetrating radar (GPR)

Yunlong Guo, Guixian Liu, Guoqing Jing, Jianjun Qu, Shilei Wang & Weile Qiang

To cite this article: Yunlong Guo, Guixian Liu, Guoqing Jing, Jianjun Qu, Shilei Wang & Weile Qiang (2022): Ballast fouling inspection and quantification with ground penetrating radar (GPR), International Journal of Rail Transportation, DOI: 10.1080/23248378.2022.2064346

To link to this article: https://doi.org/10.1080/23248378.2022.2064346

Published online: 11 Apr 2022.

INTERNATIONAL JOURNAL OF RAIL TRANSPORTATION
https://doi.org/10.1080/23248378.2022.2064346

Ballast fouling inspection and quantification with ground penetrating radar (GPR)

Yunlong Guo[a], Guixian Liu[b], Guoqing Jing[c], Jianjun Qu[b], Shilei Wang[b] and Weile Qiang[b]

[a]Faculty of Civil Engineering and Geosciences, Delft University of Technology, Delft, Netherlands; [b]Infrastructure Inspection Research Institute, China Academy of Railway Sciences Co., Ltd, Beijing, China; [c]School of Civil Engineering, Beijing Jiaotong University, Beijing, China

ABSTRACT

Ground penetrating radar (GPR) has been applied for ballast layer inspection for two decades, mainly for the analysis of ballast layer fouling levels. However, some issues that affect the inspection quality remain unsolved, such as issues involving the GPR equipment quality (antenna) and the correlation between the GPR indicator and fouling index. With the aim of solving these two issues, in this paper, we investigated the difference between the results of two different antennas, the GPR data processing technique, indicators for the fouling level (by GPR signal processing) and the correlation between the indicators and fouling index (obtained by sieving). The results show that the antenna quality determines the inspection quality. The indicators can reflect the ballast layer fouling level, and they correlate the best with the fouling index (obtained by the percentage of particles passing through a 5 mm sieve size). This study is helpful for the future modification of railway ballast maintenance standards.

ARTICLE HISTORY
Received 17 December 2021
Revised 4 April 2022
Accepted 6 April 2022

KEYWORDS
Ground penetrating radar; GPR; railway ballast; track inspection; ballast fouling; track geometry

1. Introduction

Ballast layer is the crucial component for ballasted track geometry with a train speed of 200–250 km/h [1,2]. The track irregularity under train speeds of 200–250 km/h mostly results from ballast layer differential deformation [3]. Under train cyclic loadings (after a long service time), the possibility of ballast layer differential deformation gradually increases, and the ballast layer gradually loses its elasticity and drainage [4–6]. The track geometry is maintained/corrected by frequent maintenance work (tamping, stabilization) [7], and finally, ballast cleaning and renewal must be performed [8,9].

The performance of the ballasted track is mostly determined by the ballast layer condition, while fouling (also named contamination) in the ballast layer is a key factor in determining the condition of the ballast layer [10,11]. In addition, ballast fouling is the reason why ballast layers need to be cleaned and replaced by new ballast [12,13]. First, poor drainage is caused by clogging of the voids in the ballast layer by fouled ballast [14], forming mud pumping [15,16]. The fouled ballast mixed with rain water becomes lubrication for the ballast layer, as proven in [17–19], and the mixture reduces the shear strength of the ballast layer by 40% [18,20]. Second, ballast fouling also reduces the resistance from the ballast layer to the sleeper, which causes track instability and irregular track geometry (e.g., rail buckling) [21–23]. Lateral resistance is important to maintain track stability and geometry and maintain ride comfort and safety [24]. Last, the fouled ballast layer loses elasticity,

CONTACT Guixian Liu liuguixian@rails.cn Infrastructure Inspection Research Institute, China Academy of Railway Sciences Co., Ltd, Daliushu 2, Haidian District, Beijing, China

especially in some special areas (cold regions, wind-blown sand regions) where the ballast layer is rapidly fouled [25,26]. In addition, vegetation easily grows on the fouled ballast layer, causing potential danger to the trains [27]. Ballast cleaning and renewal have large labour and money costs [28].

Due to the limited developments in track inspection equipment and technology, the current ballast layer condition is mostly assessed by indirect means through the total passing gross load [8]. For example, in China, the current regulation for ballast layer maintenance stipulates that the ballast cleaning and renewal cycle should be mainly determined by the passing gross load with the complement of the fouling index (through in-site digging and sieving) at the mud-pumping location [29]. Fouling mainly occurs inside the ballast layer; it develops first in the bottom = ballast layer and gradually accumulates to reach the top ballast layer. Fouling also occurs in the subballast layer and subgrade layer due to the high pressure between ballast and subgrade/subballast [30,31]. Fouling is very difficult to observe until mud pumping occurs, especially in pluvial regions (e.g., Netherlands) [32]. Therefore, inspecting ballast fouling and quantifying the fouling level at an early stage are crucial.

More importantly, ballast fouling sources are influenced by many factors [2], such as the gross passing load, ballast material, transportation type (freight or passenger), weather, and environment, for which ballast fouling and the corresponding ballast layer degradation are very difficult to predict [33]. Therefore, performing ballast layer maintenance using only a simple factor is not reasonable, especially as the train speed and freight load keep increasing.

To solve this problem, ground penetrating radar (GPR), a non-destructive inspection technique, has been used to evaluate ballast layer conditions, especially for quantifying ballast fouling. During the past 20 years, a rapidly increasing number of studies have been performed involving many aspects of ballast fouling [34–46], as summarized below.

- Evaluating ballast fouling by the dielectric constant of the ballast layer. In [36], clean ballast was mixed with different percentages of soil as fouling (0% – 24%), and at these fouling percentages, the dielectric permittivity values measured were between 3.51 and 5.35. In [47], the dielectric permittivity was confirmed under the condition that more fouling sources (sand, gravel) and percentages (0% – 50%) were mixed with clean ballast, demonstrating that the dielectric permittivity can be used to reflect the ballast fouling level. However, one dielectric permittivity value can be caused by many situations, e.g., fouling sources and water content [48]. In addition, to calculate the dielectric permittivity from radar signals, it is necessary to know where the reflective interface is, i.e., the ballast layer thickness. The expected results, such as the fouling types, the water content and the actual thickness of the reflective interface, cannot be obtained, and they still need to be obtained by in situ digging and laboratory analysis.
- Evaluating ballast fouling through the time domain and frequency domain of the GPR signal. In [26], ballast fouling is evaluated by the frequency domain, which was converted from the time domain using the Fourier transform. In [49], scatter analyses were performed on GPR signals (time domain) to reflect the fouling level, including area, axis crossing and inflexion point analyses. In addition, this study found that bowtie antennas at 500 MHz can provide fouling index results at a higher correlation coefficient (0.92). In [12], the GPR signal (time-domain) was decomposed into several levels of wavelet decomposition based on wavelet transform. The standard deviation of the wavelet coefficients (scattering intensity of the GPR signal) was used to reflect the fouling level. In [50], migration and time-to-depth conversion were studied, and both time-domain and frequency-domain signal processing techniques were applied.
- A linear correlation was created between the indicator (GPR signal analysis result) and the fouling level based on the low-frequency GPR signal at approximately 500 MHz, while the relationship based on the medium- and high-frequency antennas at 1–2 GHz tends to be more

complex and shows a high regression phenomenon. This phenomenon may also result from the limited number of samples. GPR signals were collected mostly in dry fields or indoor environments, and the GPR signals of the water-containing ballast layer in the natural environment are not yet correlated with the fouling level. To ensure the applicability of GPR, the relationship between the GPR signal and the radar signal indicator needs to be established in conjunction with the ballast grading (particle size distribution; PSD) and railway line type. The methods for calculating ballast degradation and the fouling index in different countries vary due to the different requirements of diverse standards, such as those for the ballast material and PSD.

- Evaluating ballast fouling through the change in the scattering pattern. This evaluation is based on high-frequency air-coupled antenna (1–2 GHz), using which different ballast fouling levels clearly showing different scattering patterns [51]. In addition, the ballast layer thickness, ballast fouling level and amount of stored water can be evaluated. The scattering source is named scatter. The scatters in ballast layers are the air voids. With this technique, the track geometry irregularity is correlated with the fouling level of the ballast layer [51–53]. Three indices were created, as follows: the ballast depth exceedance, ballast fouling index and percentage void contamination.
- Although analysing scattering patterns of high-frequency GPR signals have been validated in laboratory and field tests, research on the effects of ballast moisture on the scattering patterns is still lacking. Note that the correlation between the GPR signal and the fouling level was mostly established without considering the ballast moisture level. In addition, how to distinguish the different types of fouling needs more study, e.g., dedicated coal transport lines where the fouling material is predominantly fine-grained coal.

In summary, the use of the GPR technique for evaluating ballast layer conditions is becoming mature. The thickness of the clean ballast layer can be measured based on the 2 GHz GPR radar scattering signal. In situ sieving results were mostly used to calibrate the fouling level of the ballast layer. The thickness of the clean ballast can be used to assess the drainage capacity of ballast layer. The ballast fouling level can be used to guide ballast cleaning and renewal.

However, insufficient studies have been performed using the GPR technique to correlate multiple types of GPR results with multiple types of fouling indices, especially in diverse field railway lines. It is important to measure more locations under complex environmental conditions, such as weather and transportation types. In addition, China is a large area with multiple complex regions, soft subgrade areas, earthquake areas, mountainous areas, desert areas, etc., which provides a very good opportunity to compare the ballast layer conditions, analyse ballast fouling and contribute to maintenance strategies.

This paper has two objectives with regard to presenting the GPR results of diverse ballast layers in different regions, with the aim of supplementing the standard for GPR application for ballast layer inspection:

(1) Develop indicators that can accurately correlate the ballast fouling level with GPR results (main objective);
(2) Check how the different antennas affect the GPR inspection results of the ballast fouling level.

2. Methodology

First, the GPR information applied in this study is introduced. Second, the method for developing the ballast layer fouling level index with GPR signals is explained. Third, the tested railway lines are introduced, including the transportation type, yearly passing gross load, railway line classification, special structures (tunnel or bridge) and sleeper types. Finally, to the method for calculating and measuring the fouling level with the field ballast is introduced.

2.1. Ground penetrating radar

2.1.1. GPR equipment

The applied GPR was produced by the Geophysical Survey Systems, Inc. company and included two 2 GHz air-coupled antennas and a data collection unit. The data collection setting for the unit has a time range of 15 ns. The antennas are suspended in the air from a hand-towed railway cart at two heights of approximately 400 mm and 190 mm from the ballast surface. The 190 mm height is also used and tested because in the future, it is the lowest possible height when installing GPR equipment in the inspection train. The antennas were suspended above the ballast shoulder to collect GPR data on the position that usually generates the most fouling after long-term operation. The cart speed is approximately 3 km/h. The GPR equipment setup is shown in Figure 1.

In addition, the performances of different brands of HF antennas were also compared in our study. The comparison details are described in Table 1. Note that the test railway line in the table is the location where the comparison of the two antennas was performed. In the table, section marks K154 + 700 and 160 + 230 are the line marks, which represent the start position and end position, respectively. Based on the section mark, the length of the railway line section can be calculated. The railway line length for comparing the two antennas was approximately 15 km. In the table, to distinguish between the lines in the double-line railway, one is named the upstream line, and the other is named the downstream line. This was stipulated by the China Railway International Co Ltd. The railway line is marked with, e.g., '#1', to distinguish between the different railway lines, as explained in Table 2.

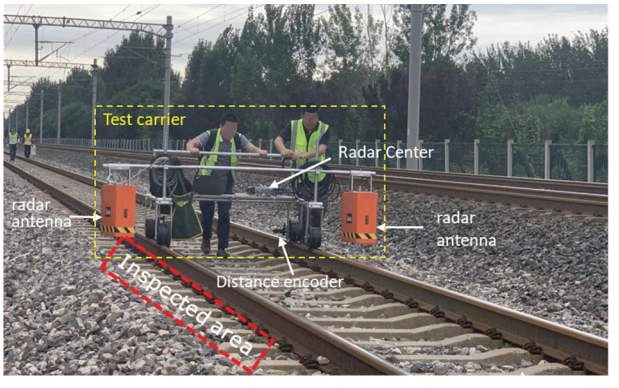

Figure 1. GPR equipment on a ballasted track using a 2 GHz antenna.

Table 1. Test description.

Test railway line	Railway line #2 (passenger and freight mixed line), approximately 15 km distance, section mark: K154 + 700–160 + 230
Total gross passing load	Double railway lines: 92 Mt upstream; 56 Mt downstream
Maintenance	Upstream line was cleaned in 2021; Downstream line has not cleaned for nearly 10 years
Antennas for comparison	US GSSI 2 GHz air-coupled antenna; 2 GHz air-coupled antenna (made in Shandong Province)
Acquisition parameters	15 ns time range; 5 cm channel spacing
Test time	November 2021
Environmental conditions	There was no rainfall three days before the test.

Table 2. Tested railway lines and line conditions.

No.	Line name	Length (km)	Date of test	Gross passing load (Mt)	Year of last cleaning
1	Line #1	3.6	2021/5/24	26	2009
2	Line #2	5.5	2021/11/10	92	2021
3		5.5	2021/11/9	56	2010
4	Line #3	1.1	2021/11/3	24	-
5		1.3	2021/11/4	13	-
6		1.3	2021/11/4	13	-
7	Line #4	9.0	2021/6/7	-	2013
8	Line #5	9.8	2021/8/27	450	2020
9	Line #6	13.0	2021/10/20	17	-
10		13.0	2021/10/21	17	-
11		3.0	2021/10/22	17	-
12		3.0	2021/10/22	17	-

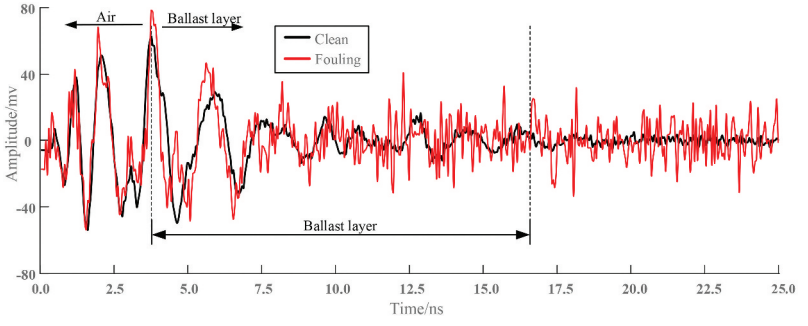

Figure 2. GPR signals (time-domain) of the clean and fouled ballast layers.

2.1.2. Basic principle of GPR signals

One example of the obtained field data during ballast layer inspection is used to show the GPR signal differences between the clean ballast layer and fouled ballast layer (Figures 2 and 3). The two sections of the ballast layer are in the same railway line but different sections, which were cleaned and renewed in 2018 and 2010, respectively. A typical single-channel waveform is shown in Figure 2. The effective number of signal inflexion points that are inside the clean ballast layer is approximately 260. The dielectric constant is calculated by 6, and the corresponding signal travel depth is approximately 77 cm. In most cases, the thickness of the ballast layer is at most 55 cm, which means that the GPR signal can meet the needs of ballast layer detection. By comparing the two figures in Figure 2, the obvious difference between the signals of the fouled ballast layer is their high frequency signal, and the number of axis crossings is significantly increased. The power spectrum of the two signals after fast Fourier transform (FFT) is shown in Figure 3. This shows that the power spectrum of the clean ballast layer approaches zero after a 2 GHz frequency. For most frequencies, the power spectra of the fouled ballast layer are higher than those of the clean ballast layer.

2.2. GPR data processing technique

2.2.1. Scatter analyses of GPR signals

The significant GPR signal differences (in the time and frequency domains) between the clean and fouled ballast layers may reflect the ballast fouling level. In this paper, based on both the time and frequency domains, the correlations between five indicators and the ballast fouling level are studied. The five indicators are the feature area (SfRa; FFT), scan area (StAb), axis crossings (CrossNum), inflection points (InflecNum) and feature area (Hilbert transform), as shown in Figure 4. The

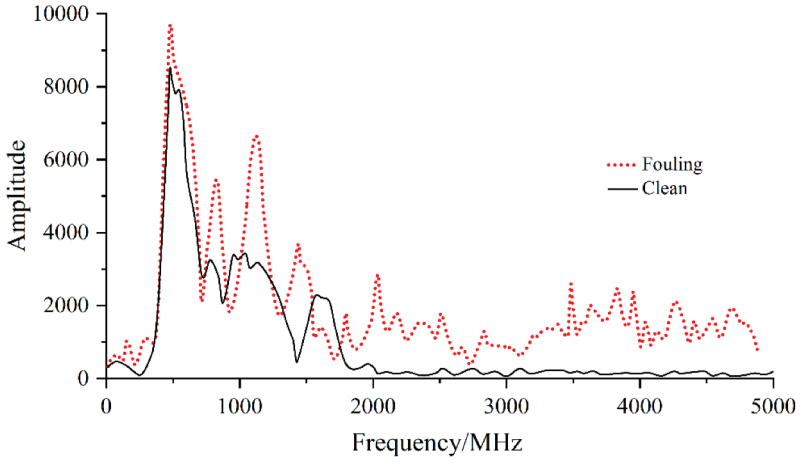

Figure 3. GPR signal spectra (frequency domain) of the clean and fouled ballast layers.

featured area is calculated by the integration of signals. One (SfRa) is processed by converting time-domain signals to frequency-domain signals with the FFT. The other (HhtAb) converts time-domain signals to time-domain signals with the Hilbert transform.

2.2.2. Processing method

With the GPR signal data, the processing method consists of the following three steps: (1) data matrix establishment, (2) determining the useful data (signal in ballast layer) and (3) converting these data into indicators (to reflect the fouling level). The method for processing the signal and obtaining the StAb is explained through an example in the following paragraphs.

(1) Data matrix establishment.

We extracted raw data matrix P, which has a total of n rows m columns of data composition. n indicates the radar total points (forming the received signal, Figure 5. Note that the points are the traditional air removal filter in the time domain, and in the process, no new sampling is implemented.), which was 512 in most studies. m is the total channel number, and the adjacent channel distance along the railway line direction is Δd, which can be set through the GPR equipment. The value of Δd used in the ballast layer studies was in the range of 5–20 cm. mΔd is the length of the tested railway line.

(2) Determining the useful data.

The first wave peak of the signal indicates signal (points) in the ballast layer. In addition, the ballast-air interface can also be identified based on the distance of the antenna from the ballast layer surface and the signal travel speed. The starting point at the wave peak is extracted and recorded as sr, which divides the signal into two parts, i.e., air and ballast, as shown in Figure 5. Afterwards, the air part of the signal is removed, and a new matrix for the ballast layer (PI) is created. sr+1 to n rows of points are used to form the matrix PI, which consists of l rows and m columns, l = n − sr.

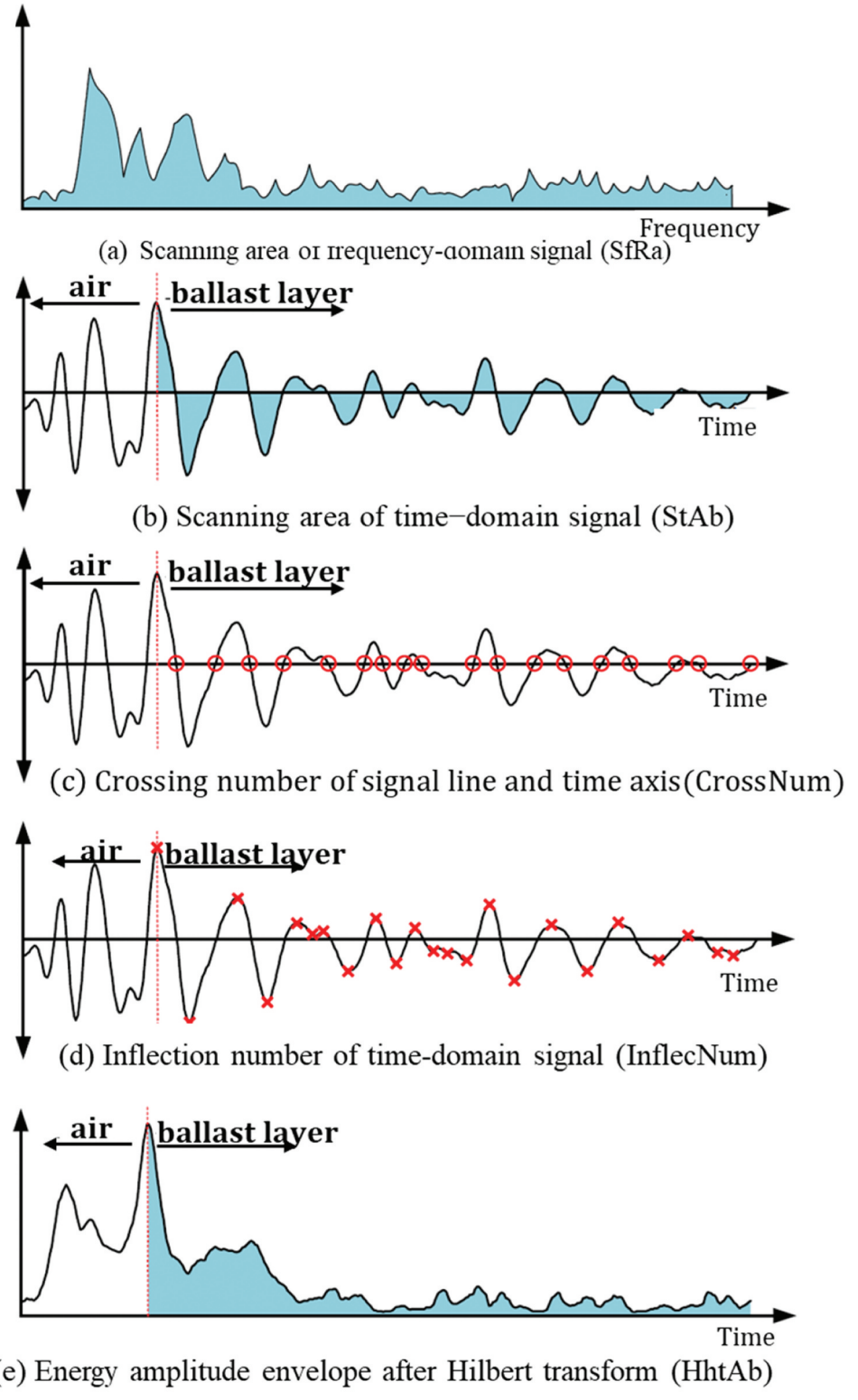

Figure 4. Fouling level indicators obtained by GPR signal data processing.

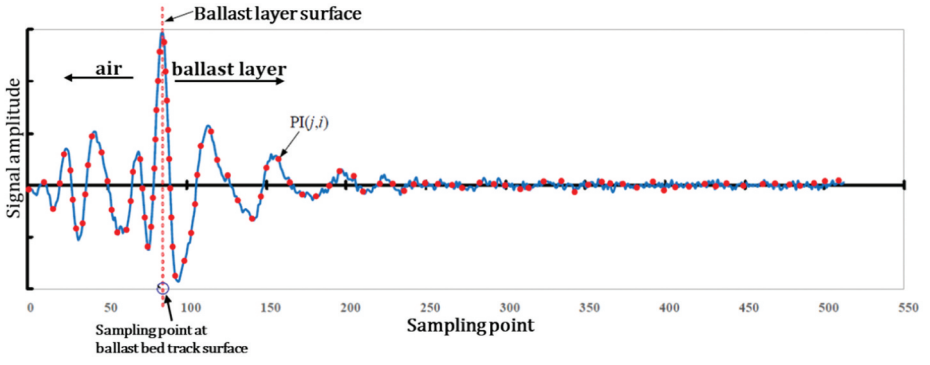

Figure 5. Extraction of points composing the GPR signal.

(3) Converting the signal data into indicators.

The absolute value of the signal amplitude is integrated along the time axis as the characterization value of the current channel. All channels form a sequence of characterization values, StAb. The sequence StAb contains m elements, and the ith element is StAb(i), where $1 \le i \le m$. StAb(i) is formed by the integration of the *i*th column of the matrix PI (j,i) along the time axis, where $1 \le j \le l$ The flowchart for solving the sequence of StAb eigenvalues based on the matrix PI is shown in Figure 6. In the figure, Δt is the time difference between adjacent rows, which can be calculated from the GPR system time range (T). The value of the time window, T, is generally in the range of 15 ~ 25 ns, $\Delta t = T/(n-1)$, and n is the number of points.

Note that the same processing procedure was applied for the other indicators. The Hilbert transform of a continuous time signal x(t) is equal to the output response xh(t) after the signal has been passed through a linear system with impulse response $h(t) = 1/\pi t$. After the Hilbert transform, the amplitude of each frequency component in the frequency domain remains the same, but the phase will be shifted by 90°. This means that the signal is lagged by $\pi/2$ for positive frequencies and led by $\pi/2$ for negative frequencies; hence, the Hilbert transform is also known as a 90° phase shifter. The Hilbert transform is used to describe the envelope, instantaneous frequency and instantaneous phase of amplitude modulation or phase modulation, which makes the analysis easy and has important theoretical and practical value in communication systems. In communication theory, the Hilbert transform is a tool for analysing signals, and in digital signal processing, it can be used not only for signal transformation but also for filtering, and different types of Hilbert filters can be made. A more detailed explanation of the Hilbert transform can be found in [54].

2.2.3. Indicator validation

To verify the proposed indicators, the GPR inspection results are used. The railway line used for comparing the indicators is Line #3 K36 + 828 – K36 + 852 (clean ballast layer) and K38 + 248 – K38 + 272 (fouled ballast layer), where each section length is 24 m (approximately 40 sleepers). The effectiveness of the five indicators is studied, as shown in Figure 7. The figure shows that the 5 indicators increase in the fouled/dirty ballast layer compared to the clean ballast layer, which means they can be used to reflect the ballast fouling level. Combining the results from our other studies (draft with the name: Comparison of fouling indices for better ballast layer fouling evaluation using ground penetrating radar (GPR)), the StAb can better reflect ballast layer fouling. The StAb will be used in this study and correlated with the fouling index (calculated by sieving results; Section 2.4.2).

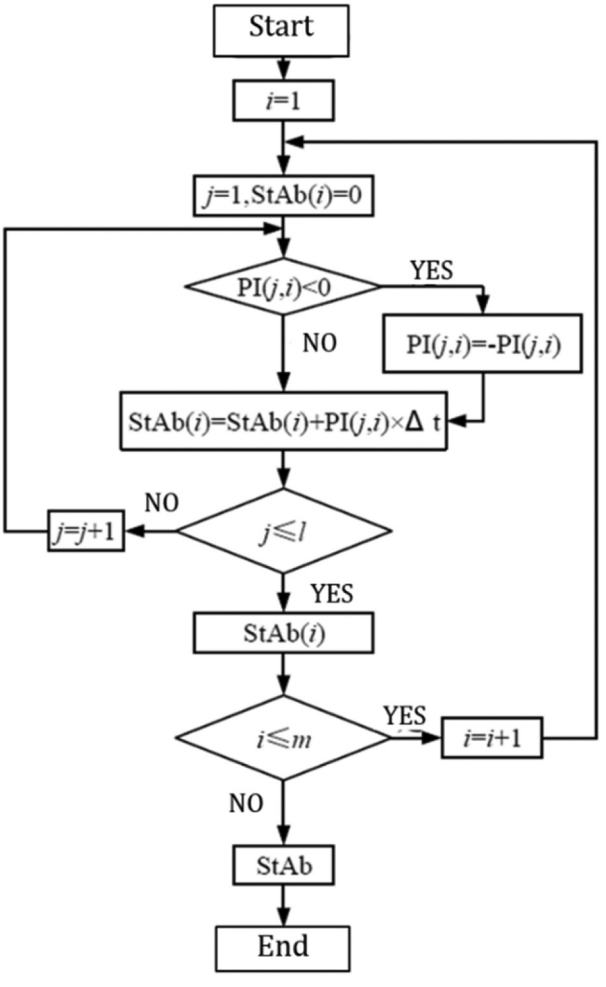

Figure 6. Flowchart of the StAb calculation.

In Figure 7(c), HhtAb-Av is the average value of HhtAb for every 2.4 m length. We applied this average value of HhtAb because the 5 cm channel spacing leads to significantly different HhtAb values (as well as the other four indicators) when the GPR equipment is placed on the sleeper and crib ballast (inspected area, Figures 1 and 8). Then, the HhtAb values have frequent fluctuations. To reduce the fluctuations, the average value of the HhtAb values every 2.4 m (4-sleeper spacing) was used as the indicator, as shown in Figure 7. HhtAb-Av presents the average value. It can be observed that this HhtAb-Av has fewer fluctuations than HhtAb.

To further validate these values, the fouling level (assessed through GPR) and the fouling level (assessed through sieving) are compared. The sieving method used to evaluate the fouling level is introduced in Section 2.4.

2.3. Railway lines for data collection

Six different railway lines, which have different line types, locations, maintenance histories and ballast layer conditions, were inspected with GPR. The railway lines cover a passenger and freight mixed line, passenger line, heavy-haul line and research test lines. The selected selections of these

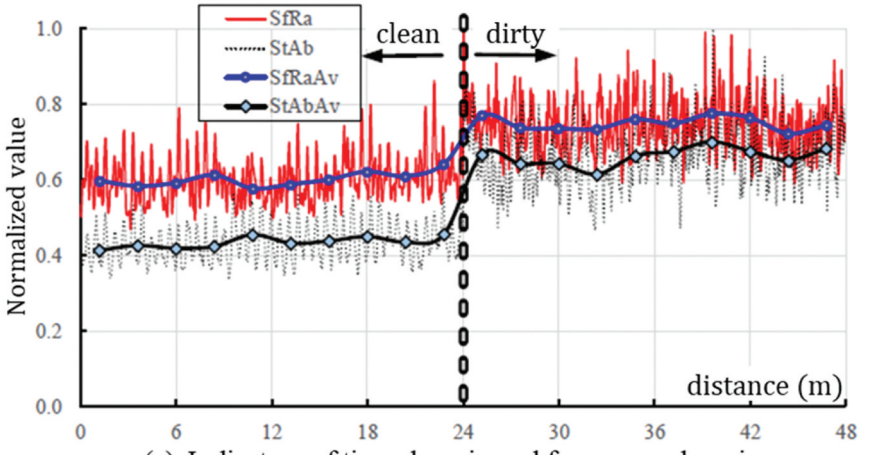

(a) Indicators of time-domain and frequency-domain signal

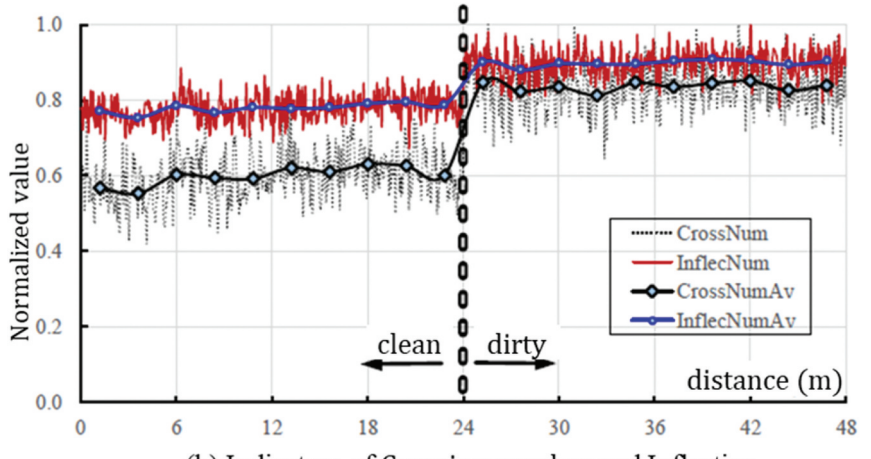

(b) Indicators of Crossing number and Inflection Number at time-domain curve

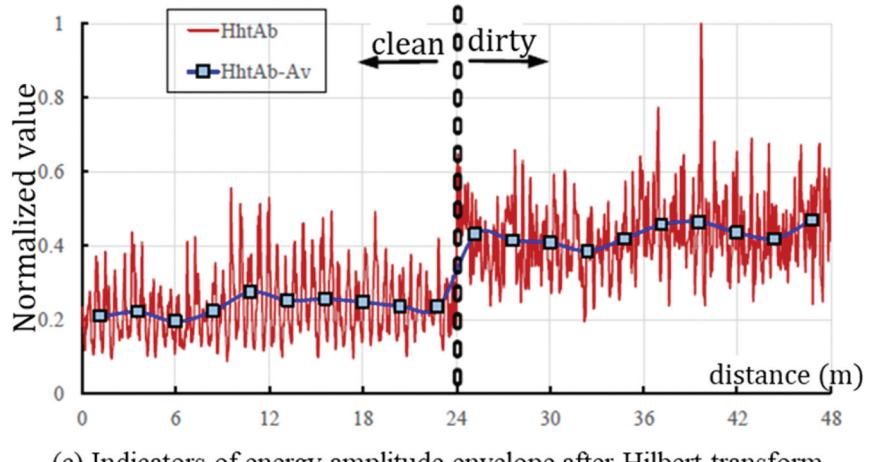

(c) Indicators of energy amplitude envelope after Hilbert transform

Figure 7. Ballast layer fouling level presented by the five indicators.

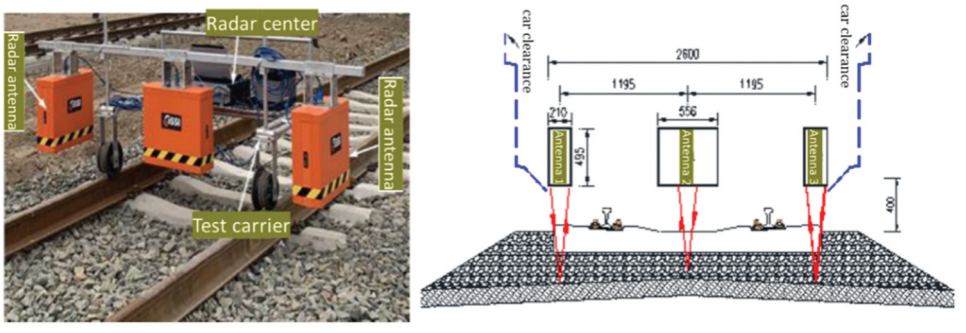

(a) GPR detection positons (b) Detection positons: shoulder and crib

Figure 8. GPR detection positions (a) GPR detection positons (b) Detection positons: shoulder and crib.

lines have different clean and renewal years. A total line length of approximately 70 km was tested, and 62 test holes were dug to obtain and assess the fouled ballast. More details can be found in Table 2.

As shown in Figure 8, the GPR detection positions are given, which are near the ballast shoulders 1.195 m from the railway line centre. A hole (size: 500 × 300 × 300 mm3) was dug at every testing point. To prevent disturbance from the surrounding ballast particles, steel sticks were placed in the ground around the hole, as shown in Figure 9.

2.4. Fouling index correlation

2.4.1. In situ samples

The method for sieving fouled ballast includes four steps.

- **Weighing the samples**. The ballast samples were collected and weighed to obtain the sample mass (m_{wet}). Then, the ballast samples were placed in a drying oven at a temperature of 100 ~ 110 degrees for 4 ~ 6 h to dry thoroughly. When the dried ballast samples reached room temperature, their dry weights (m_{dry}) were taken.

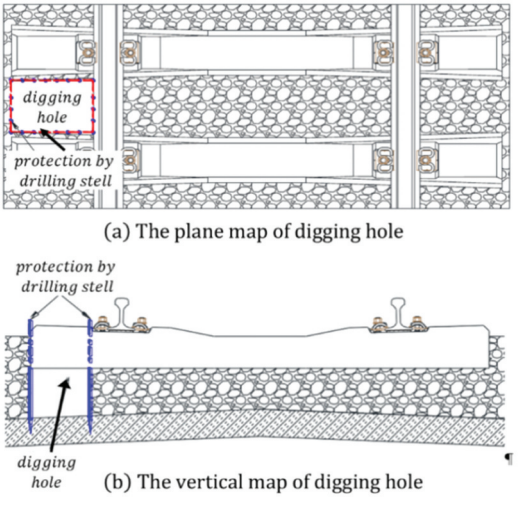

(c) Field test of excavation and sampling

Figure 9. Dug hole and steel stick demonstration.

- **Soaking samples**. A container (volume: 90 litres) was filled with 30–40 litres of clean water, and then the fouled ballast was immersed in clean water for a period of 12 hours. After the adhering materials on the ballast surface were sufficiently soaked and stirred, the clean ballast particles were removed and washed with water.
- **Sieving samples**. We dried the ballast particles (size above 5 mm) and weighed their mass. The samples were sieved with square-hole sieves, and the mass of each particle size range was determined. The fines (size below 5 mm) were dried and then sieved with sieves with 5 mm, 2.5 mm, 1.0 mm and 0.076 mm square holes. Each size was weighed and sealed for the next step of extraction.
- **Ballast density**. The ballast particles above 10 mm were washed, dried and then classified according to the rock material. Then, three ballast particles were selected from each type of rock material for density measurement.

2.4.2. Fouling indices

The fouling index based on sieving (5 mm) to reflect the fouling level is shown in the following equation. It is based on the percentage of fines and particles below 5 mm. The calculation method is the same for 10 mm and 16 mm sieves. In the equation, m_{5mm} is the weight of particles below 5 mm, and m_{all} is the total weight of the sample.

$$FI_{5mm} = \frac{m_{5mm}}{m_{all}} \tag{1}$$

3. Results and discussions

3.1. Different antennas

The scan area (StAb) was selected for comparing the antennas, and the results are shown in Figure 10. In the double line railway line, the peak value of the upstream line collected by the 2 GHz antenna of the GSSI is slightly smaller (by 15%) than that of the downstream line because the upstream line was cleaned and renewed this year (the downstream line was not). The average values of the fouling indicator of the upstream and downstream lines are basically the same. This phenomenon resulting from the gross passing load of the downstream line is much less than that of the upstream line (approximately 60% less).

Further comparison of the antennas shows that the results collected by the GSSI 2 GHz antenna have more peaks than the results collected by the Shandong 2 GHz antenna. The peaks are caused by the discrete distribution of ballast fouling. In addition, no significant distinguishing waves were found with the Shandong 2 GHz antenna, which means that antennas are very important for inspecting the ballast layer fouling levels.

3.1.1. Sieving results of fouled ballast

The sieving results of the fouled ballast are shown in Figure 11. For example, there are several particle size distribution curves in one figure because they result from different sieving tests over the same ballast particles with fouling at the same digging spot. The annual gross passing load of Line #1 was 26 Mt, and the latest sieving date was 2008. The sieving results show that the cumulative sieving rate below 25 mm is 37–53% and the cumulative sieving rate below 16 mm is 21–33%. The annual gross passing load of Line #2 is extremely low, and it was cleaned in 2010. The sieving results show that the cumulative sieving rate below 25 mm is 27–44% and the cumulative sieving rate below 16 mm is 16–24%. As stipulated in the maintenance regulation [29], cleaning and renewal should be performed when the total passing load is 600–700 Mt or the ballast layer has served for 15 years.

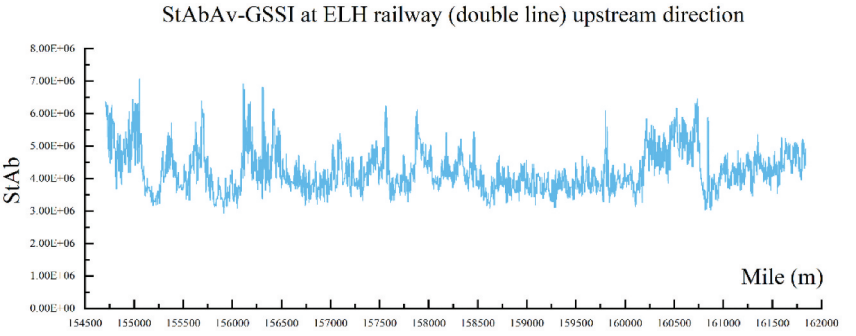

(a) 2GHz GSSI inspection at upstream line

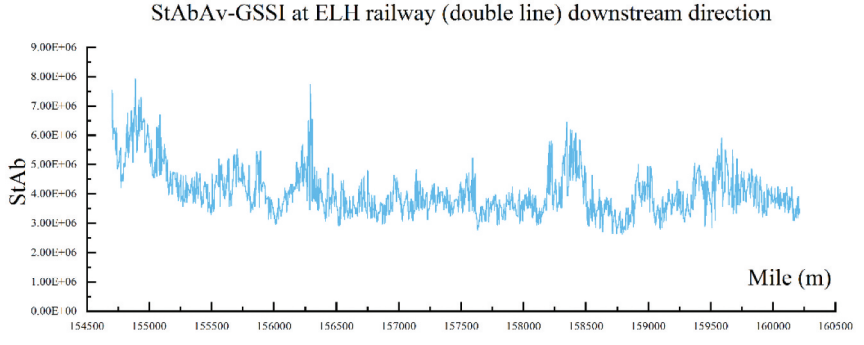

(b) 2GHz GSSI inspection at downstream line

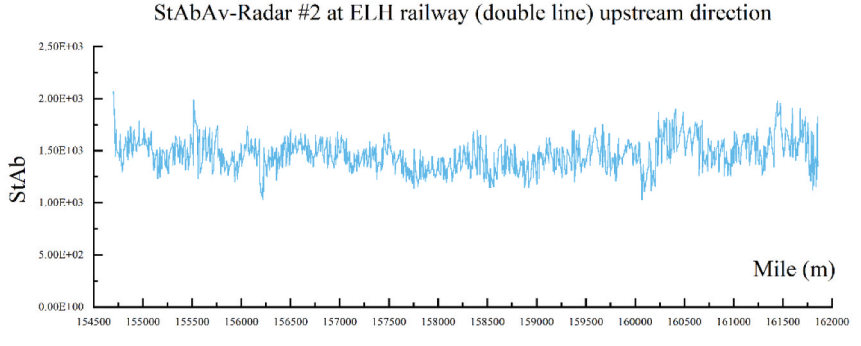

(c) 2GHz Radar #2 inspection at upstream line

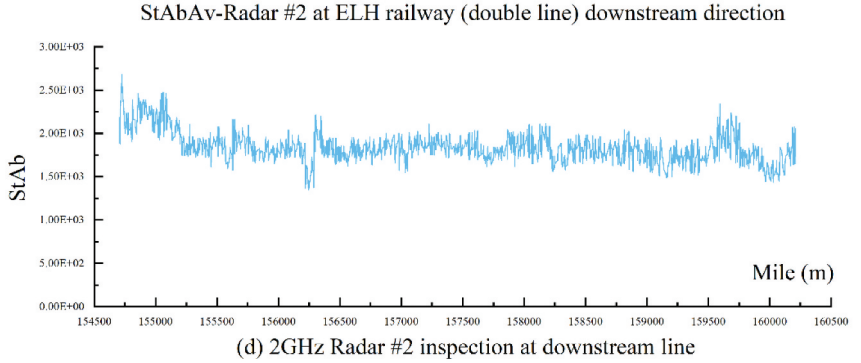

(d) 2GHz Radar #2 inspection at downstream line

Figure 10. Results of different brands of antennas with the same fouling indicator.

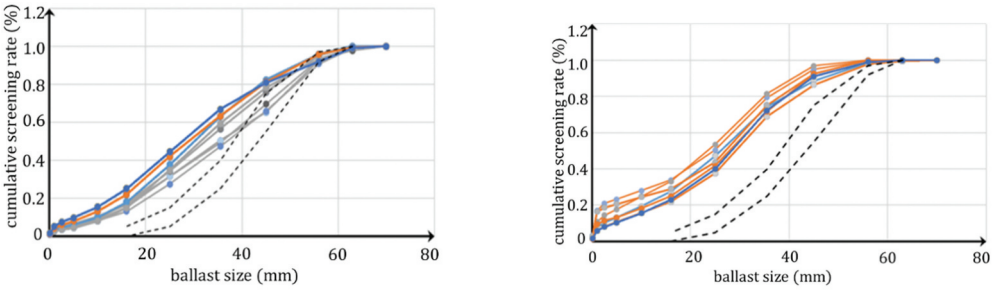

Figure 11. Sieving results of two different railway lines.

However, the sieving results show that although both the total passing load and the number of years has not met the regulation, the sieving rate below 25 mm has seriously exceeded 25%. This means that the regulation needs to be modified by adding more inspection means, especially GPR results.

3.1.2. Correlation with the GPR results

After testing the ballast layer with GPR, selected locations (in the different lines) with different StAb values were sampled and sieved to obtain the fouling index. The fouling index (passing percentage) is correlated with the fouling level indicator, StAb, as shown in Figure 12. In the figure, the y-axis of the scatter points is the StAb value, and the x-axis is the corresponding fouling index obtained by sieving. It can be observed that there is an almost linear correlation between the fouling index and StAb. As the sieve size decreases, the fouling index and StAb fit better. This demonstrates that GPR can be used as an accurate means of inspecting ballast fouling.

From the figure, it can be observed that the fouling index (obtained by passing the sample through a 5 mm sieve) correlates the best among the 5 mm, 10 mm and 16 mm sieves. However, in the maintenance regulation [29], only the fouling index (passing the 16 mm sieve percentage) was required as the indicator for ballast cleaning and renewal. Particles passing 5 mm and 10 mm are more sensitive to ballast layer fouling [55] and occupy a high percentage. More importantly, these two values can be better reflected by the GPR results. Therefore, it is recommended to use a combination of these three fouling index types (5 mm, 10 mm and 16 mm).

The following equations show the correlation between the GPR signal analysis result (StAb) and the fouling index (through sieving). In the Equations (2–4), FI_{5mm}, FI_{10mm} and FI_{16mm} are the percentages of particles passing through sieving sizes of 5 mm, 10 mm and 16 mm, respectively. They will be used in our future analysis on more ballast layers under complex conditions, such as frozen areas, mountainous areas, tunnels, bridges, etc.

$$StAb = 3.1 \times 10^5 \times FI_{5mm} + 2.9 \times 10^5 \tag{2}$$

$$StAb = 2.6 \times 10^5 \times FI_{10mm} - 4.2 \times 10^5 \tag{3}$$

$$StAb = 2.2 \times 10^5 \times FI_{16mm} - 2.0 \times 10^6 \tag{4}$$

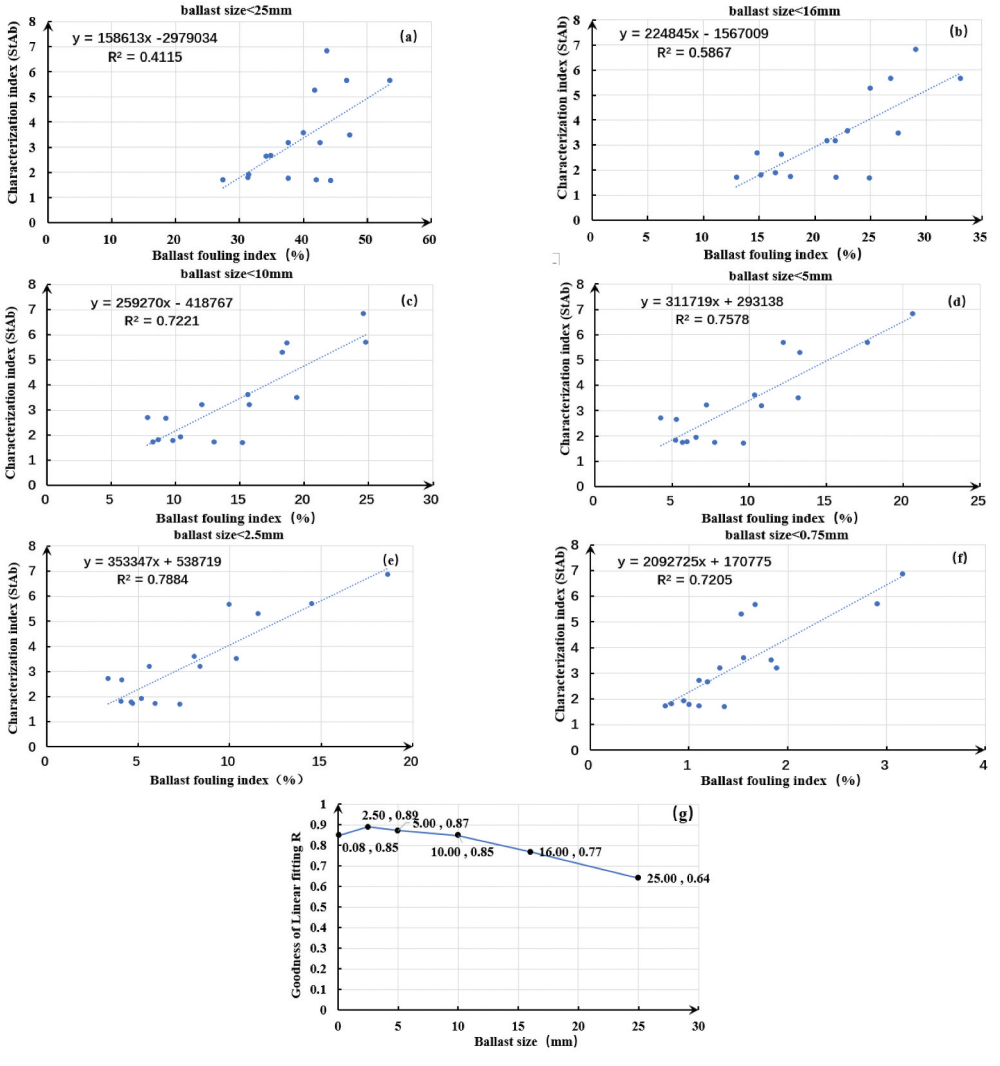

Figure 12. Linear correlation between the indicator (StAb) and the fouling index by sieving results(a ~ f: ballast sizes are respectly 25 mm, 16 mm, 10 mm, 5 mm, 2.5 mm, 0.75 mm; g: linear correlation between the indicator (StAb) and the fouling index).

4. Conclusions and perspectives

4.1. Conclusions

In this paper, ground penetrating radar (GPR) applications were the main focus. GPR was applied to the ballast layer fouling level estimation. The GPR signal processing technique and sieving fouled ballast samples are two methods used in this paper to estimate the ballast fouling level. In addition, the indicators obtained from GPR signal processing are used to reflect the fouling level. The indicators were compared with the fouling index obtained by the sieving results. After performing this study, the following conclusions are drawn.

- Compared with the 2 GHz antenna of the US GSSI company, the sensitivity of the calculated indicators of the 2 GHz antenna (Shandong company) is not high. This means that the antenna used for ballast layer inspection should be carefully selected.

- The five indicators proposed in this study, i.e., the feature area (SfRa; FFT), scan area (StAb), axis crossings (CrossNum), inflection points (InflecNum) and feature area (Hilbert transform), accurately reflect the different ballast fouling levels.
- The scan area (StAb) and feature area (Hilbert transform) are more accurate than the other indicators in terms of reflecting the ballast fouling level. The StAb correlates well with the small fouling particles.

4.2. Perspectives

We applied several indicators to indicate ballast fouling through the analysis of the GPR signal, and much data were obtained. In the next step, we will compare them and give a more accurate correlation to reflect the ballast layer condition more precisely. Over six railway lines were scanned with GPR, and their complex environmental conditions were also considered in our ballast layer condition analysis. For example, in our analysis of one railway line, it was found that the linear correlation between the GPR indicator and the fouling index (by sieving) was unclear. Through fouling material analysis, we found that there is a high amount of iron ore, which greatly influences the GPR signal.

Disclosure statement

No potential conflict of interest was reported by the author(s).

Funding

This research is funded by the Key Research and Development Project of the China Academy of Railway Sciences Corporation Limited (key research and development project of China Academy of Railway Sciences Corporation Limited 2021YJ251).

ORCID

Yunlong Guo http://orcid.org/0000-0003-4339-1833
Guoqing Jing http://orcid.org/0000-0001-9655-2229

References

[1] Zhai W. Vehicle–track coupled dynamics: theory and applications. Singapore: Springer Nature; 2020.
[2] Selig ET, Waters JM. Track geotechnology and substructure management. London: Thomas Telford; 1994.
[3] Tutumluer E, Qian Y, Hashash YM, et al. Discrete element modelling of ballasted track deformation behaviour. Int J Rail Transp. 2013;1(1–2):57–73.
[4] Indraratna B, Salim W, Rujikiatkamjorn C. Advanced rail geotechnology-ballasted track. London: CRC press; 2011.
[5] Li D, Hyslip J, Sussmann T, et al. Railway geotechnics. Boca Raton: CRC Press; 2015.
[6] Xu L, Zhai W. Train–track coupled dynamics analysis: system spatial variation on geometry, physics and mechanics. Railway Eng Sci. 2020;28(1):36–53.
[7] Bakhtiary A, Zakeri JA, Mohammadzadeh S. An opportunistic preventive maintenance policy for tamping scheduling of railway tracks. Int J Rail Transp. 2021;9(1):1–22.
[8] Guo Y, Markine V, Jing G. Review of ballast track tamping: mechanism, challenges and solutions. Constr Build Mater. 2021;300:123940.
[9] Borkovcová A, Borecký V, Artagan SS, et al. Quantification of the mechanized ballast cleaning process efficiency using GPR technology. Remote Sens. 2021;13(8):1510.
[10] Huang H, Tutumluer E. Discrete element modeling for fouled railroad ballast. Constr Build Mater. 2011;25(8):3306–3312.
[11] Indraratna B, Ngo NT, Rujikiatkamjorn C. Behavior of geogrid-reinforced ballast under various levels of fouling. Geotext Geomembranes. 2011;29(3):313–322.

[12] Shangguan P, Al-Qadi IL, Leng Z. Ground-penetrating radar data to develop wavelet technique for quantifying railroad ballast–fouling conditions. Transp Res Rec. 2012;2289(1):95–102.
[13] Ngo NT, Indraratna B, Rujikiatkamjorn C. Stabilization of track substructure with geo-inclusions—experimental evidence and DEM simulation. Int J Rail Transp. 2017;5(2):63–86.
[14] Schmidt S, Shah S, Moaveni M, et al. Railway ballast permeability and cleaning considerations. Transp Res Rec. 2017;2607(1):24–32.
[15] Wan Z, Bian X, Li S, et al. Remediation of mud pumping in ballastless high-speed railway using polyurethane chemical injection. Constr Build Mater. 2020;259:120401.
[16] Koohmishi M. Drainage potential of degraded railway ballast considering initial gradation and intrusion of external fine materials. Soils Found. 2019;59(6):2265–2278.
[17] Indraratna B, Ngo NT, Rujikiatkamjorn C. Deformation of coal fouled ballast stabilized with geogrid under cyclic load. J Geotech Geoenviron Eng. 2013;139(8):1275–1289.
[18] Indraratna B, Ionescu D, Christie HD. Shear behavior of railway ballast based on large-scale triaxial tests. J Geotech Geoenviron Eng. 1998;124(5):439–449.
[19] Indraratna B, Tennakoon N, Nimbalkar S, et al. Behaviour of clay-fouled ballast under drained triaxial testing. Geotechnique. 2013;63(5):410–419.
[20] Ngo NT, Indraratna B, Rujikiatkamjorn C. DEM simulation of the behaviour of geogrid stabilised ballast fouled with coal. Comput Geotech. 2014;55:224–231.
[21] Ngamkhanong C, Feng B, Tutumluer E, et al. Evaluation of lateral stability of railway tracks due to ballast degradation. Constr Build Mater. 2021;278:122342.
[22] Xu Y, Gao L, Zhang YR, et al. Discrete element method analysis of lateral resistance of fouled ballast bed. J Cent South Univ. 2016;23(9):2373–2381.
[23] Guo Y, Zong L, Markine V, et al. Experimental and numerical study on lateral and longitudinal resistance of ballasted track with nailed sleeper. Int J Rail Transp. 2022;10(1):114–132.
[24] Jing G, Aela P. Review of the lateral resistance of ballasted tracks. P I Mech Eng F-J Rail Rapid Transit. 2020;234(8):807–820
[25] Esmaeili M, Aela P, Hosseini A. Experimental assessment of cyclic behavior of sand-fouled ballast mixed with tire derived aggregates. Soil Dyn Earthq Eng. 2017;98:1–11.
[26] Silvast M, Nurmikolu A, Wiljanen B, et al. An inspection of railway ballast quality using ground penetrating radar in Finland. P I Mech Eng F-J Rail Rapid Transit. 2010;224(5):345–351
[27] Indraratna B, Rujikiatkamjorn C, Vinod JS, et al. A review of ballast characteristics, geosynthetics, confining pressures and native vegetation in rail track stabilisation. Transp Eng Austr. 2009;12(1):25–36.
[28] Zhao J, Chan AH, Stirling AB, et al. Optimizing policies of railway ballast tamping and renewal. Transp Res Rec. 2006;1943(1):50–56.
[29] Ltd CRIC. General railway line maintenance rules [in Chinese]. Beijing: China Railway Publishing House; 2019.
[30] Xiao J, Wang Y, Zhang D, et al. Testing of contact stress at ballast bed-soil subgrade interface under cyclic loading using the thin-film pressure sensor. J Test Eval. 2019;48(3):2104–2117.
[31] Esmaeili M, Ataei S, Siahkouhi M. A case study of dynamic behaviour of short span concrete slab bridge reinforced by tire-derived aggregates as sub-ballast. Int J Rail Transp. 2020;8(1):80–98.
[32] Kuo C, Hsu C, Chen Y, et al. Using ground-penetrating radar to promote the investigating efficiency in mud pumping disaster of railways. Proc Eng Technol Innov. 2016;4:49–51.
[33] Danesh A, Palassi M, Mirghasemi AA. Evaluating the influence of ballast degradation on its shear behaviour. Int J Rail Transp. 2018;6(3):145–162.
[34] Wang S, Liu G, Jing G, et al. State-of-the-Art Review of Ground Penetrating Radar (GPR) Applications for Railway Ballast Inspection. Sensors. 2022;22(7): 2450.
[35] Benedetto A, Benedetto F, Tosti F. GPR applications for geotechnical stability of transportation infrastructures. Nondestruct Test Eva. 2012;27(3):253–262.
[36] Benedetto A, Tosti F, Ciampoli LB, et al. Railway ballast condition assessment using ground-penetrating radar–An experimental, numerical simulation and modelling development. Constr Build Mater. 2017;140:508–520.
[37] Alani AM, Aboutalebi M, Kilic G. Applications of ground penetrating radar (GPR) in bridge deck monitoring and assessment. J Appl Geophys. 2013;97:45–54.
[38] Tosti F, Patriarca C, Slob E, et al. Clay content evaluation in soils through GPR signal processing. J Appl Geophys. 2013;97:69–80.
[39] Benedetto A, Pensa S. Indirect diagnosis of pavement structural damages using surface GPR reflection techniques. J Appl Geophys. 2007;62(2):107–123.
[40] Benedetto A, Tosti F, Ciampoli LB, et al. An overview of ground-penetrating radar signal processing techniques for road inspections. Signal Process. 2017;132:201–209.

[41] Ferrante C, Bianchini Ciampoli L, Benedetto A, et al. Non-destructive technologies for sustainable assessment and monitoring of railway infrastructure: a focus on GPR and InSAR methods. Environ Earth Sci. 2021;80 (24):1–20.
[42] Artagan SS, Bianchini Ciampoli L, D'Amico F, et al. Non-destructive assessment and health monitoring of railway infrastructures. Surv Geophys. 2020;41(3):447–483
[43] Tosti F, Ciampoli LB, Calvi A, et al. An investigation into the railway ballast dielectric properties using different GPR antennas and frequency systems. NDT E Int. 2018;93:131–140.
[44] Ciampoli LB, Tosti F, Brancadoro MG, et al. A spectral analysis of ground-penetrating radar data for the assessment of the railway ballast geometric properties. NDT E Int. 2017;90:39–47.
[45] Al-Qadi I, Xie W, Roberts R. Optimization of antenna configuration in multiple-frequency ground penetrating radar system for railroad substructure assessment. NDT E Int. 2010;43(1):20–28.
[46] Anbazhagan P, Dixit PN, Bharatha TP. Identification of type and degree of railway ballast fouling using ground coupled GPR antennas. J Appl Geophys. 2016;126:183–190.
[47] Artagan SS, Borecky V. Advances in the nondestructive condition assessment of railway ballast: a focus on GPR. NDT E Int. 2020;115:102290.
[48] Clark MR, Gillespie R, Kemp T, et al. Electromagnetic properties of railway ballast. NDT E Int. 2001;34 (5):305–311.
[49] De Bold R, O'connor G, Morrissey JP, et al. Benchmarking large scale GPR experiments on railway ballast. Constr Build Mater. 2015;92:31–42.
[50] Bianchini Ciampoli L, Calvi A, D'Amico F. Railway ballast monitoring by GPR: a test-site investigation. Remote Sens. 2019;11(20):2381.
[51] Al-Qadi IL, Xie W, Roberts R. Scattering analysis of ground-penetrating radar data to quantify railroad ballast contamination. NDT E Int. 2008;41(6):441–447.
[52] Sadeghi J, Motieyan-Najar ME, Zakeri JA, et al. Improvement of railway ballast maintenance approach, incorporating ballast geometry and fouling conditions. J Appl Geophys. 2018;151:263–273.
[53] Eriksen A, Gascoyne J, Fraser R. Ground penetrating radar as part of a holistic strategy for inspecting trackbed. Aust Geomech Soc. 2011;46(3):1.
[54] Roberts R, Al-Audi I, Tutumluer E, et al. Subsurface evaluation of railway track using ground penetrating radar. Final report. Federal Railroad Administration; 2008.
[55] Qian Y, Mishra D, Tutumluer E, et al. Characterization of geogrid reinforced ballast behavior at different levels of degradation through triaxial shear strength test and discrete element modeling. Geotext Geomembranes. 2015;43(5):393–402.